Geophysical Research Letters

RESEARCH LETTER
10.1029/2020GL091095

Special Section:
The Ice, Cloud and land Elevation Satellite-2 (ICESat-2) on-orbit performance, data discoveries and early science

Rapid Formation of an Ice Doline on Amery Ice Shelf, East Antarctica

Roland C. Warner[1], Helen A. Fricker[2], Susheel Adusumilli[2], Philipp Arndt[2], Jonathan Kingslake[3], and Julian J. Spergel[3]

[1]Australian Antarctic Program Partnership, Institute for Marine and Antarctic Studies, University of Tasmania, Hobart, TAS, Australia, [2]Institute of Geophysics and Planetary Physics, Scripps Institution of Oceanography, University of California, San Diego, La Jolla, CA, USA, [3]Department of Earth and Environmental Sciences, Lamont-Doherty Earth Observatory of Columbia University, Palisades, NY, USA

Abstract Surface meltwater accumulating on Antarctic ice shelves can drive fractures through to the ocean and potentially cause their collapse, leading to increased ice discharge from the continent. Implications of increasing surface melt for future ice shelf stability are inadequately understood. The southern Amery Ice Shelf has an extensive surface hydrological system, and we present data from satellite imagery and ICESat-2 showing a rapid surface disruption there in winter 2019, covering ~60 km^2. We interpret this as an ice-covered lake draining through the ice shelf, forming an ice doline with a central depression reaching 80 m depth amidst over 36 m uplift. Flexural rebound modeling suggests 0.75 km^3 of water was lost. We observed transient refilling of the doline the following summer with rapid incision of a narrow meltwater channel (20 m wide and 6 m deep). This study demonstrates how high-resolution geodetic measurements can explore critical fine-scale ice shelf processes.

Plain Language Summary Surface melting over Antarctica's floating ice shelves is predicted to increase significantly during coming decades, but the implications for their stability are unknown. The Antarctic Peninsula has already seen meltwater driven ice shelf collapses. We are still learning how meltwater forms, flows and alters the surface, and that rapid water-driven changes are not limited to summer. We present high-resolution satellite data (imagery and altimetry) showing an abrupt change on East Antarctica's Amery Ice Shelf in June 2019 (midwinter). Meltwater stored in a deep, ice-covered lake drained through to the ocean below, leaving a deep, uneven 11 km^2 depression of fractured ice (a "doline") in the ice shelf surface. The reduced load on the floating ice shelf resulted in flexure, with over 36 m of uplift centered on the former lake. Simple flexure modeling showed that this corresponds to about 0.75 km^3 of water being lost to the ocean. ICESat-2 observations in summer 2020 profiled a new narrow channel inside the doline as meltwater started refilling it from a new lake created by the flexure. ICESat-2's capacity to observe surface processes at small spatial scales greatly improves our ability to model them, ultimately improving the accuracy of our projections.

Key Points:

- Satellite images showed an 11 km^2 depression on Amery Ice Shelf as an ice-covered lake drained abruptly in winter 2019 forming an ice doline
- ICESat-2 and WorldView data show elevation fell as much as 80 m in the depression, amidst 60 km^2 of hydrostatic rebound and uplift over 36 m
- ICESat-2 photon data profiled a new meltwater channel, incised when a lake formed by the flexural uplift overflowed into the doline in 2020

Supporting Information:

Supporting Information may be found in the online version of this article.

Correspondence to:

R. C. Warner,
roland.warner@utas.edu.au

Citation:

Warner, R. C., Fricker, H. A., Adusumilli, S., Arndt, P., Kingslake, J., & Spergel, J. J. (2021). Rapid formation of an ice doline on Amery Ice Shelf, East Antarctica. *Geophysical Research Letters*, *48*, e2020GL091095. https://doi.org/10.1029/2020GL091095

Received 8 OCT 2020
Accepted 26 APR 2021

1. Introduction

Antarctica's ice shelves regulate the flow of grounded ice to the ocean, through a process known as buttressing (Thomas, 1979). Under stable climate conditions, ice shelves remain approximately in equilibrium, gaining mass from ice flow across the grounding line and local snowfall, and losing mass through ocean melting at their bases (year-round), iceberg calving from their ice fronts (episodic) and surface melting (principally during summer). In recent decades, some Antarctic Peninsula ice shelves have experienced greater surface melting in response to increasing atmospheric temperatures (Barrand et al., 2013; Trusel et al., 2015). This has led to more extensive melt ponds, providing sufficient water volumes to drive so-called "hydrofracturing" (Weertman, 1973), sometimes leading to ice shelf collapse via an extreme disintegrative type of calving involving multiple hydrofractures (Banwell et al., 2013; Scambos et al., 2003; van den Broeke, 2005). In these regions, flow rates of the grounded ice have increased (Rignot et al., 2004; Scambos et al., 2003), due to loss of buttressing.

Antarctic surface melting has been projected to double by 2050 (Gilbert & Kittel, 2021; Trusel et al., 2015), raising concerns about the stability of other ice shelves. This has renewed interest in monitoring surface

meltwater on all ice shelves, its capacity to pond in critical regions, and its potential to accumulate and drive ice shelf collapse through multiple hydrofractures (Bell et al., 2018; Kingslake et al., 2017; Lai et al., 2020). Other studies have observed local ice shelf flexure and fracture in response to surface meltwater transport, ponding and drainage (Banwell et al., 2019; Dunmire et al., 2020; Lenaerts et al., 2017). Despite this interest and some modeling studies (Buzzard et al., 2018a, 2018b; MacAyeal & Sergienko, 2013; Robel & Banwell, 2019), processes such as hydrofracture and flexure remain under-studied, and ice-sheet models do not yet include realistic treatment of these processes.

Significant surface melting occurs on Amery Ice Shelf in East Antarctica, mostly in its southern section (Mellor & McKinnon, 1960; Swithinbank, 1988). Meltwater accumulates and flows through extensive drainage systems that typically terminate in elongate lakes (Fricker et al., 2009; Spergel et al., 2021), sometimes also referred to as meltstreams (Phillips, 1998). Ice "dolines" (by analogy with karst landscapes) are depressions left behind after surface or englacial (buried) meltwater lakes drain through the ice shelf via hydrofracture (Mellor, 1960). Understanding doline formation is important as it provides a mechanism for surface meltwater to drain rapidly into the ocean, resulting in local mass loss and generating significant flexural stresses. Doline formation may also impact meltwater drainage system development, and satellite observations indicate that dolines can persist for decades, moving with the ice shelf flow (Fricker et al., 2002; Swithinbank, 1988). The presence of dolines on several ice shelves (Bindschadler et al., 2002; Moore, 1993) suggests that they may drain significant amounts of meltwater through hidden fractures, although this has not been quantified and the formation of a doline has not previously been observed.

In this paper, we present new observations from Landsat 8 and WorldView satellite imagery and ICESat-2 laser altimetry revealing the abrupt appearance of a major localized surface deformation of the central Amery Ice Shelf covering a total area of 60 km^2. The data suggest rapid drainage of a deep, perennially ice-covered lake in midwinter (June 2019) forming an ice doline. Analysis of ICESat-2 repeat tracks and a pair of WorldView digital elevation maps (DEMs) revealed elevation changes ranging from a net fall of 80 m beneath the former lake surface to adjacent uplift reaching 36 m. Elastic modeling of flexural rebound showed that the deformation is consistent with a loss of ~0.75 km^3 of water. The high resolution elevation data available from ICESat-2 and WorldView before and after the lake drainage event provided an unprecedented opportunity to observe doline formation and details of the associated surface meltwater features.

2. Satellite Image Observations of Amery Doline Formation

Amery Ice Shelf's surface melt system is predominantly in the southern third of the ice shelf (Figure 1a). Along both margins, melt features are confined to narrow linear surface depressions parallel to ice flow (Fricker et al., 2009; Phillips, 1998; Spergel et al., 2021). The broad central flowband, which originates from the Mellor Glacier, has a different hydrologic regime; longitudinal ridges are less controlling, and it has an additional general East to West component to its slope. Accordingly, it displays a broader lake and stream geometry with significant catchment areas focused into major meltstreams and lakes at the western side of the flowband (Figure 1a).

Examination of visible satellite imagery (Landsat 8 and Sentinel-2) acquired in January 2020, serendipitously revealed a striking collapsed surface structure within the Mellor flowband, which we interpret as the formation of an ice doline (Figure 1c). We used a variety of satellite images (see the Supporting Information) to explore the timing and structure of the collapse feature, primarily visible imagery, but also synthetic aperture radar (SAR). Multi-spectral imagery (MODIS, Landsat 8 and Sentinel-2) uses passive sensors and is available only when the sun is high enough, from October to March (austral summer), and is also affected by clouds. Sentinel-1 SAR uses an active sensor allowing year-round, all-weather acquisition, extending observation capability into the winter and through cloudy periods.

Visible imagery before and after winter placed the surface deformation event between March 31, 2019 and September 14, 2019, and Sentinel-1 SAR imagery further constrained it to the interval June 5–11. Images from the previous melt season (2018/2019; e.g., Figure 1b) showed that the location coincided with a largely ice-covered lake of ~20 km^2 which is part of the surface hydrologic system mapped by Spergel et al. (2021). Prior to drainage, approximately 11 km^2 of the lake had a perennial ice cover, with a corrugated surface and extensive "scar" features. Seasonally, an arm of open water at the southern end received meltwater

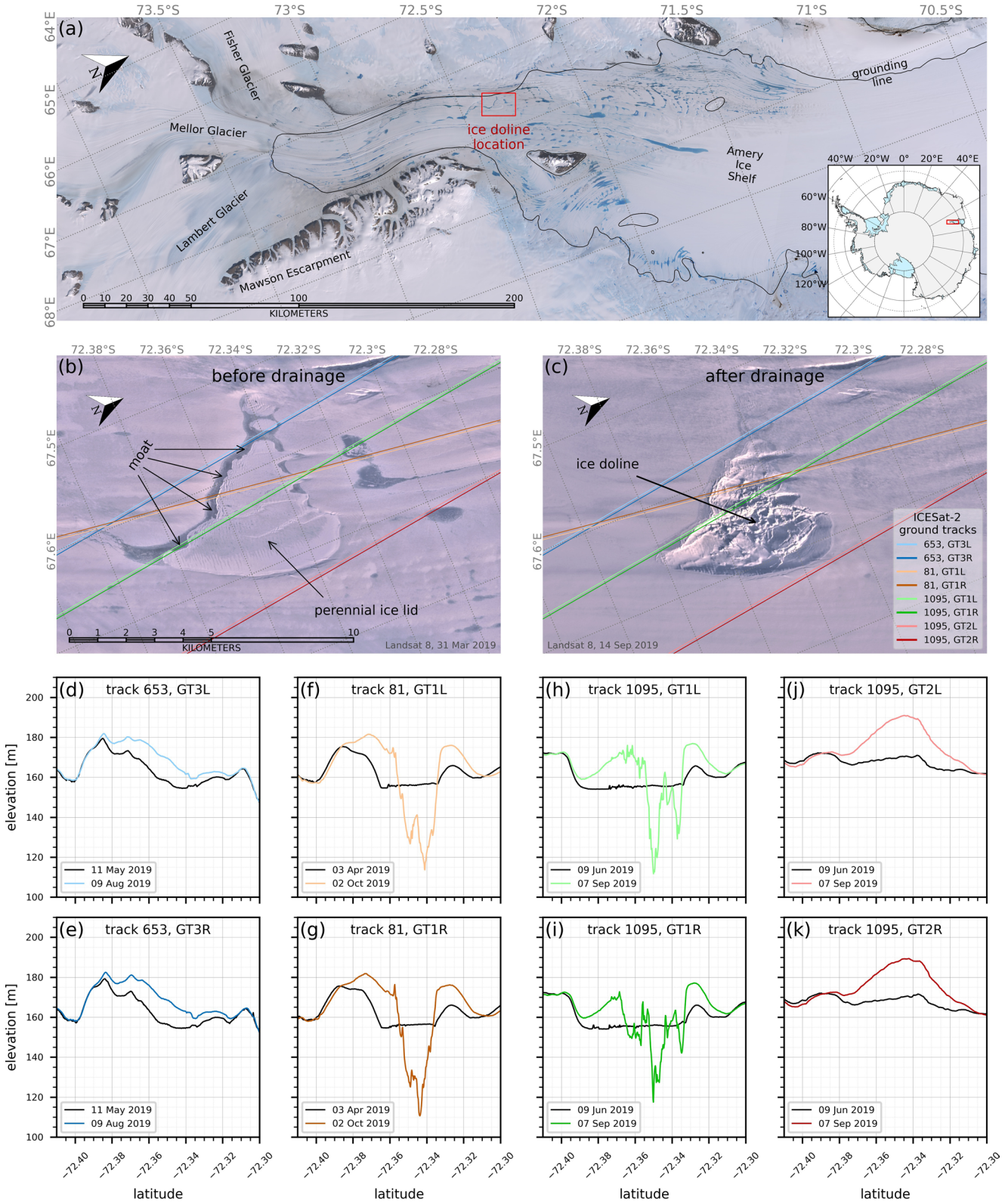

Figure 1. Formation of doline on Amery Ice Shelf. (a) Landsat 8 image over the southern Amery Ice Shelf on January 17, 2019; Landsat 8 images for (b) March, 31 and (c) September 14, 2019, with color-coded ICESat-2 ground tracks (GTs) overlaid; (d–k) ICESat-2 ATL06 data for repeats of GTs (from west to east) before and after doline formation.

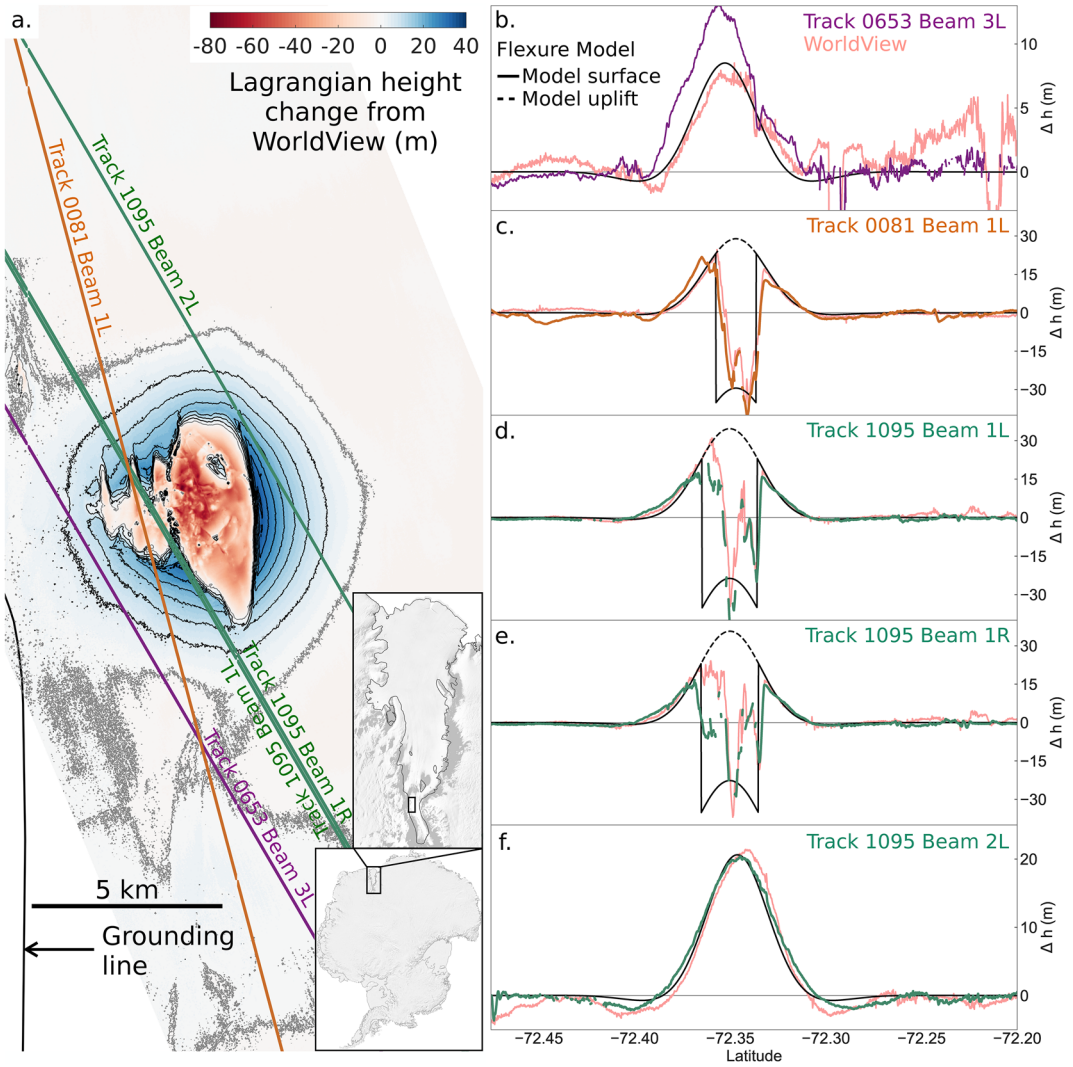

Figure 2. Elevation changes and estimation of unloading by the drainage event. (a) Elevation changes for the doline and surrounding ice shelf from Lagrangian differencing of WorldView digital elevation maps (DEMs) (March 26, 2018 and December 20, 2019). Contours are shown for positive changes: 5 m interval, zero contour in grey, overlaid with locations of ICESat-2 ground tracks (GTs). (b–f) ATL06 elevation difference profiles along ICESat-2 GTs (from west to east), with corresponding profiles from the WorldView DEM difference and flexural modeling. Imagery © 2020 DigitalGlobe, Inc.

via a single channel from an extensive surface drainage system of interconnected ponds and streams (Figure 1a). From this arm, a shallow, sinuous channel (or "moat") of open water extended along the southern shore, fringing the ice lid, while other isolated regions of open water appeared along the northern shore (Figure 1b).

The collapse structure (Figure 1c) displays many of the characteristics of another doline on Amery Ice Shelf, described by Mellor and McKinnon (1960). We see a broad region of subsidence containing both broken slabs of ice and clear traces of the previous ice surface and lake shore. The image reveals that the lake had four parallel elongated basins (see also Figure 2a), with the eastern one clearly the largest. Near the lake margins, particularly around the main eastern basin, the ice lid has subsided, essentially intact, to the lakebed and surface corrugations remain visible. Over the interior, the lid has broken into slabs, with some suggestion of fracturing over local bathymetric highs. Shadows in the imagery indicate that the ice lid had considerable thickness. Along the southern shore the "moat" and the edge of the ice lid remain intact as a

border to the subsidence, suggesting that the ice lid extended just beyond the deeper parts of the lake into shallow marginal areas.

We examined older imagery to explore the history and evolution of the lake, extending the time series used in Spergel et al. (2021). Using visible imagery from Landsat 4, 5, 7 (1972–1974, 1988–1992, 1999 to 2013), Landsat 8 (2013–2020) and Sentinel-2 A/B (2015–2020), we tracked the main basin of the lake back to 1973. The basin has evolved during its advection with the ice flow, including deformation by ice motion and rearrangement of water ponding in the three smaller western basins. The corrugated ice lid has been present since 1973 which, combined with the persistence of the scar features, suggests that this was the first significant drainage event during this period.

3. Topographic Signature of Doline Formation

To quantify the deformation associated with the doline formation, we examined elevation data spanning the event. We combined precise, high-resolution repeat elevation profiles from ICESat-2 satellite laser altimetry with broader spatial coverage from differencing digital elevation maps generated from WorldView satellite stereo image pairs.

3.1. Surface Elevation Profiles (ICESat-2)

We used surface elevation data from NASA's ICESat-2, which was launched in September 2018. ICESat-2 carries the Advanced Topographic Laser Altimeter System (ATLAS), a photon-counting, 532 nm (green) lidar. ATLAS splits the transmitted laser pulse into six beams, configured as three pairs, each containing one weak and one strong beam (separated by 90 m); each pair is separated by 3.3 km. For each beam, the footprint diameter is ~11 m and along-track distance between footprints is 0.7 m. Over ice sheets, ICESat-2 operates with the central beam pair following a reference ground track (RGT); each beam follows its own ground track (GT; named GT1R, GT1L, GT2R, ... to GT3L). Extending to latitudes ±88°, the 1,387 RGTs form a complete cycle that is repeated every 91 days.

We used two ICESat-2 data products: Full photon clouds (ATL03; Neumann et al., 2019, 2020) and the Land Ice Along-Track Height Product (ATL06; Smith et al., 2019, 2020). ATL03 photons are geolocated and assigned a confidence of representing the surface (high, low or medium). ATL03 data are useful here due to the high spatial resolution along-track, and because they can be used to retrieve estimates of depths of surface water, since photons may reflect from both the water and the bottom of a melt lake at the same location (Fair et al., 2020; Fricker et al., 2020). ATL06 data are derived from ATL03 data and contain WGS-84 elevations 20 m apart, averaged along 40 m overlapping segments, for a single reflecting surface, optimized for ice (Smith et al., 2019). For ice sheets, ICESat-2 has demonstrated elevation retrieval precision to better than 13 cm (one standard deviation) for both ATL03 and ATL06 data, based on calibration field experiments on the Antarctic plateau at the 88°S limit where multiple orbits converge (Brunt et al., 2019, 2021).

We initially used the open-source software OpenAltimetry (https://openaltimetry.org; Khalsa et al., 2020), and examined all available ICESat-2 tracks over the Amery doline region. Four ICESat-2 RGTs cross the region (Figures 1b and 1c). Two GT's of Track 1095 had repeats immediately before (June 9, 2019) and 3 months after (September 11, 2019) the lake drainage and doline formation, capturing a significant disruption in the surface elevations centered on 72.35°S, 67.66°E (Figures 1h–1k). The event was also captured on Tracks 0081 and 0653 (Figures 1d–1g). Tracks 1095 GT1R and L (Figures 1h and 1i) showed that the lake and its ice cover were intact at 00:06:20 June 9, 2019, further constraining the lake drainage event duration to less than 70.35 h between June 9 and 11, 2019. ICESat-2 repeat measurements showed elevations lowered as much as ~46 m in the center of the doline; post-collapse, the maximum range of elevations over the former lake was ~66 m (Figure 1g).

3.2. Surface Elevation Changes (ICESat-2 and WorldView)

ICESat-2: Accurate elevation differences can be determined for ICESat-2 exact repeat tracks, although they contain a signal from ice advection. To quantify changes associated with doline formation, we used ATL06 data for the GTs that had repeats spanning the event. We observed significant elevation changes along four

unique RGTs (eight individual GTs; five examples are shown in Figure 2b–2f). For Tracks 0653 and 1095 data come from successive cycles, minimizing the effect of ice motion, whereas Track 0081 repeats were two cycles apart.

WorldView: To map the full spatial extent of elevation change associated with the surface deformation and complement the ICESat-2 elevation profiles, we used a pair of 16-m (downsampled from 2-m) gridded DEMs generated from stereographic pairs of high resolution (0.31 m) WorldView satellite imagery acquired at two epochs: March 26, 2018 and December 20, 2019. These DEMs were generated by Polar Geospatial Center using the SETSM software (Noh & Howat, 2017) employed for the Reference Elevation Model of Antarctica DEM (Howat et al., 2019).

We calculated elevation differences by advecting the pre-drainage DEM to coincide with the post-drainage one using ice velocities from NASA MEaSUREs ITS_LIVE project (Gardner et al., 2018, 2019). The elevation changes (Figure 2a) extended the mapping of the doline surface deformation beyond the sampling of the ICESat-2 tracks and allowed us to determine the area of subsidence where the lake drained (~11 km^2), with an average surface elevation decrease of 24 m, and a maximum decrease of 80 m. Surrounding the central depression is an area of raised elevations where differences reach +36 m. Beyond 5 km from the center of the doline the elevation change is small (typically <1 m), indicating both that the changes are localized around the doline and that uncertainties in elevation changes associated with the DEMs are much smaller than the signal.

This pattern of elevation change is consistent with flexural response of the floating ice shelf to the drainage event: Maximum uplift is centered on the greatest unloading (the lake), tapering outside the unloading region to small downward displacement beyond ~5 km, before decaying away at even greater distances (Figure 2). The region of net subsidence reveals where the void created by lake drainage exceeded flexural uplift. The entire disturbance covered ~60 km^2, which is smaller than expected from the elastic flexure scale for ice 1,450 m thick, and the amplitude of the uplift is correspondingly larger than a simple elastic response would predict. This is presumably because our observations range 2–6 months after the drainage event, and such a deflection involves a prompt elastic response and a slower, on-going response involving viscous deformation (e.g., Banwell and MacAyeal, 2015; MacAyeal et al., 2015).

4. Flexural Response of Ice Shelf to Water Lost via Lake Drainage

The observed flexural uplift of the ice shelf indicates that a significant mass loss occurred with the drainage of the englacially stored meltwater. Elevation changes over the ~11 km^2 area of net subsidence (i.e., the deep lake where the WorldView DEM difference is negative) represent a volume of 266×10^6 m^3, but this does not allow for uplift of the former lake bed. Applying a conservative estimate of this uplift (30 m) to the same area, based on elevation changes just outside the margins of the former lake, suggests an additional water loss of at least ~330×10^6 m^3, for a total of ~600×10^6 m^3.

We also used simple thin-plate elastic flexure modeling of the "hydrostatic rebound" response to unloading the ice shelf (e.g., Lambeck & Nakiboglu, 1980; MacAyeal & Sergienko, 2013) to estimate the mass loss required to cause the observed uplift. We considered the response to unloading of an axisymmetric lake with a cylindrical profile, which is expressible in terms of Kelvin functions (Lambeck & Nakiboglu, 1980), located at the centroid of the DEM difference uplift contours. We used a representative regional ice thickness of 1,450 m, from an independent DEM from Adusumilli et al. (2020), as the uniform thickness of the elastic plate. We varied Young's modulus (which represents the elastic stiffness of the ice) to match the spatial scale of the observed deflections, and varied the radius and depth of the cylindrical lake to produce amplitudes consistent with the elevation-difference profiles from ICESat-2 and the WorldView DEMs (Figure 2). This model fit corresponds to a Young's modulus of 50 MPa, and a cylindrical lake of radius 2,000 m and depth 60 m; this provides another estimate for the volume of water lost during lake drainage: 750×10^6 m^3.

Several authors (e.g., Banwell et al., 2019; Mosbeux et al., 2020; Schmeltz et al., 2002; Vaughan, 1995) have noted that modeling ice shelf elastic flexure often requires a smaller radius of flexural stiffness than expected from standard values for the Young's modulus for ice and the nominal ice thickness. In the present situation, as in Mosbeux et al. (2020), using a very low Young's modulus allows elastic modeling to

approximately match profiles that actually result from combined viscous and elastic deformations; essentially by reducing the elastic stresses in the modeled force balance. This mimics the cumulative effect of continuing viscous deformation (not modeled here), which reduces the proportion of the total surface deflection that still represents elastic deformation several months after the abrupt lake drainage event (c.f., Banwell & MacAyeal, 2015). Taking the modeled uplift simply as an empirical fit to extrapolate across the region of subsidence, the volume between that surface and the elevation differences displayed in Figure 2a (considering only regions where the modeled uplift exceeds the observed elevation changes) provides another estimate for the volume of lost water of $\sim 660 \times 10^6$ m^3.

5. Summer 2019/2020: First Melt Season in the Disrupted Hydrologic Landscape

Satellite imagery and ICESat-2 data from the 2019/2020 melt season provided an opportunity to examine the influence of the doline on the surface drainage system. A January 29, 2020 Landsat 8 image (Figure 3a) revealed meltwater in the doline and in a new lake basin. This lake (which we call the "rebound" lake) formed as the flexural uplift (see profiles in Figures 1h and 1i) isolated the southern arm of the original lake (compare with Figures 1b and 1c) and was fed by meltwater from the same catchment. The imagery and post-drainage WorldView DEM show that the sill of this lake, at the edge of the doline depression, consists of the remnants of the ice lid.

Meltwater accumulated rapidly in the rebound lake, starting around January 16, 2020 (from MODIS imagery). We estimated meltwater depths by applying Moussavi et al. (2020) light-attenuation method to Landsat 8 imagery with attenuation coefficients found empirically by Pope et al. (2016). We averaged the water depths calculated from the Landsat 8 red (B4) and panchromatic bands (B8) and integrated them to estimate volumes in the rebound lake. Volume reached 5.3×10^6 m^3 by January 18, and 8.2×10^6 m^3 by January 20, as the water level approached the sill. Based on the WorldView DEM, we estimate that the maximum capacity of this lake was approximately 15×10^6 m^3. Around January 24, 2020 (from MODIS) the rebound lake started to overflow into the doline, cutting a channel through the sill and producing distinct narrow meltwater channels within the doline that terminated in a small lake or moulin (Figure 3a).

Approximately five days after overflow commenced, Landsat 8 imagery from January 29, 2020 (Figure 3c) and ICESat-2 data from Track 0523 GT3R on January 30, 2020 (Figure 3f), captured the partial refilling of the doline; ICESat-2 indicated that the water surface in the deepest part of the doline was at 104.5 m elevation (WGS-84). Comparison of this Landsat image with the post-drainage WorldView DEM indicated water depths of up to ~30 m in that part of the doline with a volume of $\sim 5 \times 10^6$ m^3. From the Landsat 8 data, the corresponding light-attenuation estimate for the rebound lake volume on January 29 was 2.65×10^6 m^3, a net loss of 5.5×10^6 m^3 since January 20. Landsat 8 imagery from February 03 showed even more water in the doline (estimated by comparison with the DEM as $\sim 8 \times 10^6$ m^3), while the corresponding volume of the rebound lake from the light-attenuation method was 3.1×10^6 m^3.

ICESat-2 ATL03 data from Track 0523 GT3R on January 30, 2020 also captured a narrow, steep-sided drop in surface elevation (40 m along track) at −72.378° with strong scattering 3 m below the adjacent ice surface, where the near-coincident imagery (Landsat 8, January 29, 2020) showed the meltwater channel associated with the rebound lake overflow incised into the ice surface (Figure 3b). The relative orientations imply a 20 m channel width. We interpret this photon scattering (Figure 3d) to be from the water surface: There is additional scattering, likely from the ice below, but this is noisy because the water is flowing. The difference between these two surfaces (corrected for refractive index) implies a water depth of 3 m (Fricker et al., 2020). This demonstrates the ability of ICESat-2 ATL03 data to extract process-scale information relevant to surface hydrology. Although the melt channel is discernible in the corresponding ATL06 data (Figures 3d and 3e), that product does not fully resolve its detailed shape and structure.

Landsat 8 imagery for February 12 and 14, 2020 revealed a partial drainage of water from the doline suggesting re-activation of the fracture. The volumes in the rebound lake continued to decrease (to 1.44×10^6 m^3 and 0.95×10^6 m^3 respectively) although water depth determinations were increasingly hampered by surface freezing. In the next repeat of ICESat-2 Track 0523 GT3R (April 29, 2020) no water surface was visible; instead, the bed of the doline was visible at several locations, as deep as 100 m (indicated in Figure 3f).

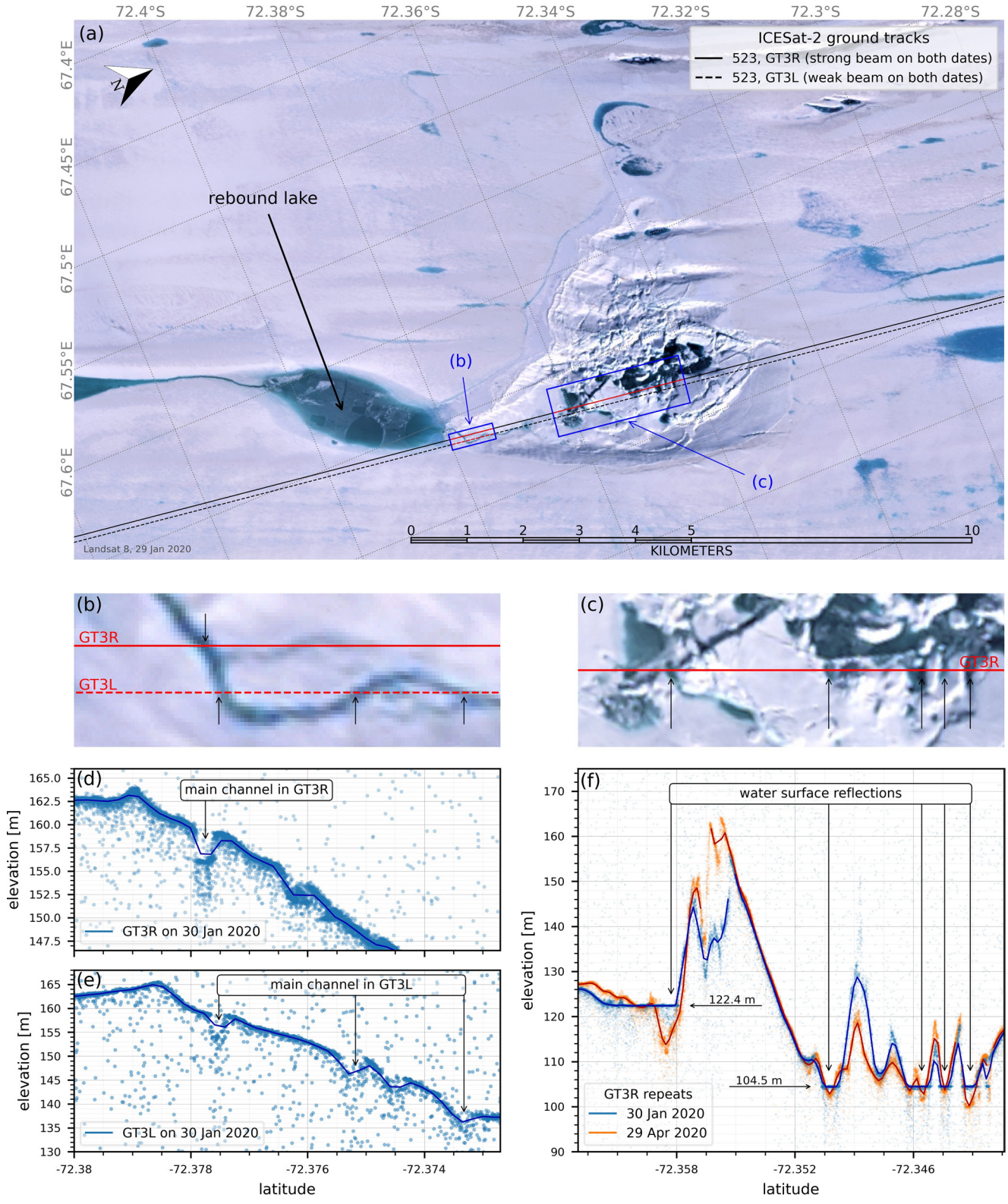

Figure 3. First melt season after doline formation (2019/2020). (a) Landsat 8 image January 29, 2020 #126/111; ICESat-2 Tracks 0523 GT3L and GT3R are shown; (b and c) zooms of Landsat 8 image; ICESat-2 ATL03 and ATL06 data (d and e) for Track 0523 GT3L and GT3R across a drainage channel (at −72.378°) incised by meltwater flow from the rebound lake to the doline; (f) for Track 0523 GT3R across the doline in January and April 2020 showing the structure of the collapsed ice lid and meltwater surfaces at 122.4 and 104.5 m; the April track is displaced to align major features with the January profile.

This is approximately 4.5 m below the water level observed in the January 30 ICESat-2 data confirming the partial drainage.

6. Implications of Lake Drainage

The lake drainage event involved the loss of an estimated 600–750 × 10^6 m^3 of water, which was delivered directly to the sub-ice-shelf cavity through 1,450 m of ice. This is many times the average annual meltwater input to the originating lake and represents an exceptional hydrological event. For comparison, this is half the amount of water injected into the Ross Ice Shelf cavity during the 2004–2006 drainage of Subglacial Lake Engelhardt (Fricker et al., 2007), but over days instead of years. The sudden injection of a buoyant plume of freshwater into the cavity ∼5 km from the lateral grounding line (Fricker et al., 2009, Figure 2), may temporarily increase local melt rates (Adusumilli et al., 2020; Jenkins, 2011).

Doline formation may lead to a significant local change in the ice shelf surface hydrology. Two opposing mechanisms are at play: Flow capture and flow diversion. In flow capture, temporarily opening an englacial pathway to the ocean makes the doline a hydropotential low, capturing local meltwater flow. In Greenland, lake drainage following hydrofracture leads to moulin formation (Das et al., 2008), which can produce internally drained catchments (Yang & Smith, 2016). On an ice shelf it could truncate drainage system growth, preventing delivery of water downstream to areas even more vulnerable to hydrofracture (e.g., Lai et al., 2020). In flow diversion, flexural uplift of the ice shelf creates a local hydropotential high, diverting meltwater flow around the newly created englacial pathway and delivering it to more vulnerable areas downstream. George VI Ice Shelf may provide examples of flow diversion, where satellite observations reveal that the flanks of dolines that have persisted for decades in areas that undergo significant meltwater ponding remain conspicuously water free (e.g., MacAyeal & Sergienko, 2013).

In the present case, despite the extensive rebound, the doline still captures the meltwater flow. We note that much of the summer 2019/2020 meltwater inflow was subsequently lost, suggesting some reactivation of the pathway to the ocean. Given the uncertainty whether it will drain to the ocean regularly or return to being a terminal lake accumulating meltwater, this doline requires continuous monitoring with ICESat-2 and satellite imagery.

7. Summary

We have used high-resolution satellite imagery, digital elevation maps based on satellite stereo photogrammetry and repeat-track ICESat-2 data (20-m land ice height product (ATL06) and full resolution photon clouds (ATL03)) to conduct a detailed process-scale analysis of a rapid lake drainage event on Amery Ice Shelf, East Antarctica in midwinter (June 9–11, 2019). The drainage of englacially stored meltwater to the ocean below left behind an ice doline, with ∼11 km^2 of local surface elevation lowering (averaging −24 m, peak value −80 m), at the center of a ∼60 km^2 region all undergoing uplift due to flexural rebound following the loss of the water loading. Uplift adjacent to the central depression reached +36 m. Simple estimates, and fitting using an elastic flexure model, showed that the magnitude and scale of flexure were consistent with the loss of a mass load equivalent to 600–750 × 10^6 m^3 of water, much larger than the average annual meltwater input to the originating lake.

The high-density, precise elevations available from ICESat-2 provided an opportunity to explore the processes associated with the formation of the doline in unprecedented detail, demonstrating that high-resolution satellite data can significantly advance our understanding of localized ice shelf processes at the scales required (10–100 m) to follow evolving ice-shelf surface hydrology and local fracture. In this case, we have been able to quantify the evolution of a significant surface drainage event on an Antarctic ice shelf. This will help to constrain models of supraglacial channel incision (e.g., Kingslake et al., 2015), ice-shelf flexure (e.g., MacAyeal & Sergienko, 2013; MacAyeal et al., 2015), and hydrofracture (e.g., Lai et al., 2020), ultimately improving assessments of the vulnerability of ice shelves to collapse.

Data Availability Statement

ICESat-2 data are available at NSIDC (https://nsidc.org/data/icesat-2). Satellite imagery is available at: USGS GloVis (https://glovis.usgs.gov/), USGS EarthExplorer (https://earthexplorer.usgs.gov/), sentinel-hub's Playground and EO Browser (https://www.sentinel-hub.com/) and ESA's Copernicus Open Access Hub (https://scihub.copernicus.eu/). See Supporting Information for details. The ITS_LIVE ice velocities (Gardner et al., 2019) are available at NSIDC (https://nsidc.org/apps/itslive/). All data and code needed to produce the figures in this document are available on Zenodo: http://doi.org/10.5281/zenodo.4747428.

Acknowledgments
We would like to thank the ICESat-2 Science Team, particularly the Land Ice group, and the OpenAltimetry Team. We are grateful to Mike Cloutier, Polar Geospatial Center for assistance with WorldView imagery and DEMs produced using data from DigitalGlobe Inc. Geospatial support for this work was provided by Polar Geospatial Center under NSF-OPP awards 1043681 and 1559691. The authors thank Alison Banwell and another anonymous reviewer for suggestions that improved the flow of the paper, and also thank Alison for a dialog that clarified our perspective on the viscoelastic character of the flexural response to the mass loss during lake drainage. The US-based authors were supported through various NASA and NSF awards: Fricker (NASA ICESat-2 ST Award No. 80NSSC20K0977); Adusumilli (NASA Earth and Space Science Fellowship (NESSF) Award No. 80NSSC18K1424); Arndt (Future Investigators in NASA Earth and Space Science and Technology Award No. 80NSSC20K1666); Spergel and Kingslake (National Science Foundation Grant No. OPP-1743310). This project received grant funding from the Australian Government as part of the Antarctic Science Collaboration Initiative program. This research was done during COVID-19 work-from-home orders in Australia and the USA; interactions were facilitated by Zoom and Slack.

References

Adusumilli, S., Fricker, H. A., Medley, B., Padman, L., & Siegfried, M. R. (2020). Interannual variations in meltwater input to the Southern Ocean from Antarctic ice shelves. *Nature Geoscience*, *13*, 616–620. https://doi.org/10.1038/s41561-020-0616-z

Banwell, A. F., MacAyeal, D., & Sergienko, O. (2013). Breakup of the Larsen B Ice Shelf triggered by chain reaction drainage of supraglacial lakes. *Geophysical Research Letters*, *40*(22), 5872–5876. https://doi.org/10.1002/2013GL057694

Banwell, A. F., & MacAyeal, D. R. (2015). Ice-shelf fracture due to viscoelastic flexure stress induced by fill/drain cycles of supraglacial lakes. *Antarctic Science*, *27*(6), 587–597. https://doi.org/10.1017/S0954102015000292

Banwell, A. F., Willis, I. C., Macdonald, G. J., Goodsell, B., & MacAyeal, D. R. (2019). Direct measurements of ice-shelf flexure caused by surface meltwater ponding and drainage. *Nature Communications*, *10*, 730. https://doi.org/10.1038/s41467-019-08522-5

Barrand, N. E., Vaughan, D. G., Steiner, N., Tedesco, M., Kuipers Munneke, P., Van den Broeke, M. R., & Hosking, J. S. (2013). Trends in Antarctic Peninsula surface melting conditions from observations and regional climate modeling. *Journal of Geophysical Research: Earth Surface*, *118*(1), 315–330. https://doi.org/10.1029/2012JF002559

Bell, R. E., Banwell, A. F., Trusel, L. D., & Kingslake, J. (2018). Antarctic surface hydrology and impacts on ice-sheet mass balance. *Nature Climate Change*, *8*, 1044–1052. https://doi.org/10.1038/s41558-018-0326-3

Bindschadler, R., Scambos, T. A., Rott, H., Skvarca, P., & Vornberger, P. (2002). Ice dolines on Larsen Ice Shelf, Antarctica. *Annals of Glaciology*, *34*, 283–290. https://doi.org/10.3189/172756402781817996

Brunt, K. M., Neumann, T. A., & Smith, B. E. (2019). Assessment of ICESat-2 ice sheet surface heights, based on comparisons over the interior of the Antarctic ice sheet. *Geophysical Research Letters*, *46*(22), 13072–13078. https://doi.org/10.1029/2019GL084886

Brunt, K. M., Smith, B. E., Sutterley, T. C., Kurtz, N. T., & Neumann, T. A. (2021). Comparisons of satellite and airborne altimetry with ground-based data from the interior of the Antarctic ice sheet. *Geophysical Research Letters*, *48*, e2020GL090572. https://doi.org/10.1029/2020GL090572

Buzzard, S., Feltham, D., & Flocco, D. (2018a). A mathematical model of melt lake development on an ice shelf. *Journal of Advances in Modeling Earth Systems*, *10*(2), 262–283. https://doi.org/10.1002/2017MS001155

Buzzard, S., Feltham, D., & Flocco, D. (2018b). Modelling the fate of surface melt on the Larsen C Ice Shelf. *The Cryosphere*, *12*(11), 3565–3575. https://doi.org/10.5194/tc-12-3565-2018

Das, S. B., Joughin, I., Behn, M. D., Howat, I. M., King, M. A., Lizarralde, D., & Bhatia, M. P. (2008). Fracture propagation to the base of the Greenland Ice Sheet during supraglacial lake drainage. *Science*, *320*(5877), 778–781. https://doi.org/10.1126/science.1153360

Dunmire, D., Lenaerts, J. T. M., Banwell, A. F., Wever, N., Shragge, J., Lhermitte, S., et al. (2020). Observations of buried lake drainage on the Antarctic Ice Sheet. *Geophysical Research Letters*, *47*, e2020GL087970. https://doi.org/10.1029/2020GL087970

Fair, Z., Flanner, M., Brunt, K. M., Fricker, H. A., & Gardner, A. (2020). Using ICESat-2 and Operation IceBridge altimetry for supraglacial lake depth retrievals. *The Cryosphere. 14*, 4253–4263. https://doi.org/10.5194/tc-14-4253-2020

Fricker, H. A., Allison, I., Craven, M., Hyland, G., Ruddell, A., Young, N., et al. (2002). Redefinition of the Amery Ice Shelf, East Antarctica, grounding zone. *Journal of Geophysical Research: Solid Earth*, *107*(B5). ECV 1-1–ECV 1-9. https://doi.org/10.1029/2001jb000383

Fricker, H. A., Arndt, P., Brunt, K. M., Datta, R. T., Fair, Z., Jasinski, M. F., et al. (2020). ICESat-2 meltwater depth estimates: Application to surface melt on southern Amery Ice Shelf, East Antarctica. *Geophysical Research Letters*, *48*, e2020GL090550. https://doi.org/10.1029/2020GL090550

Fricker, H. A., Coleman, R., Padman, L., Scambos, T. A., Bohlander, J., & Brunt, K. M. (2009). Mapping the grounding zone of the Amery Ice Shelf, East Antarctica using InSAR, MODIS and ICESat. *Antarctic Science*, *21*(5), 515–532. https://doi.org/10.1017/s095410200999023x

Fricker, H. A., Scambos, T., Bindschadler, R., & Padman, L. (2007). An active subglacial water system in West Antarctica mapped from space. *Science*, *315*, 1544–1548. https://doi.org/10.1126/science.1136897

Gardner, A. S., Fahnestock, M. A., & Scambos, T. A. (2019) [downloaded October 2019]. ITS_LIVE Regional Glacier and Ice Sheet Surface Velocities. Data archived at National Snow and Ice Data Center. https://doi.org/10.5067/6II6VW8LLWJ7

Gardner, A. S., Moholdt, G., Scambos, T., Fahnestock, M., Ligtenberg, S., van den Broeke, M., & Nilsson, J. (2018). Increased West Antarctic and unchanged East Antarctic ice discharge over the last 7 years. *The Cryosphere*, *12*(2), 521–547. https://doi.org/10.5194/tc-12-521-2018

Gilbert, E., & Kittel, C. (2021). Surface melt and runoff on Antarctic ice shelves at 1.5°C, 2°C, and 4°C of future warming. *Geophysical Research Letters*, *48*, e2020GL091733. https://doi.org/10.1029/2020GL091733

Howat, I. M., Porter, C., Smith, B. E., Noh, M.-J., & Morin, P. (2019). The reference elevation model of Antarctica. *The Cryosphere*, *13*(2). https://doi.org/10.5194/tc-13-665-2019

Jenkins, A. (2011). Convection-driven melting near the grounding lines of ice shelves and tidewater glaciers. *Journal of Physical Oceanography*, *41*(12), 2279–2294. https://doi.org/10.1175/jpo-d-11-03.1

Khalsa, S. J. S., Borsa, A., Nandigam, V., Phan, M., Lin, K., Crosby, C., et al. (2020). Open Altimetry-rapid analysis and visualization of Spaceborne altimeter data. *Earth Science Informatics*, 1–10. https://doi.org/10.1007/s12145-020-00520-2

Kingslake, J., Ely, J. C., Das, I., & Bell, R. E. (2017). Widespread movement of meltwater onto and across Antarctic ice shelves. *Nature*, *544*(7650), 349–352. https://doi.org/10.1038/nature22049

Kingslake, J., Ng, F., & Sole, A. (2015). Modelling channelized surface drainage of supraglacial lakes. *Journal of Glaciology*, *61*(225), 185–199. https://doi.org/10.3189/2015jog14j158

Lai, C., Kingslake, J., Wearing, M. G., Chen, P.-H. C., Gentine, P., Li, H., et al. (2020). Vulnerability of Antarctica's ice shelves to meltwater-driven fracture. *Nature*, *584*, 574–578. https://doi.org/10.1038/s41586-020-2627-8

Lambeck, K., & Nakiboglu, S. M. (1980). Seamount loading and stress in the ocean lithosphere. *Journal of Geophysical Research*, *85*(B11), 6403–6418. https://doi.org/10.1029/JB085iB11p06403

Lenaerts, J. T. M., Lhermitte, S., Drews, R., Ligtenberg, S. R. M., Berger, S., Helm, V., et al. (2017). Meltwater produced by wind–albedo interaction stored in an East Antarctic ice shelf. *Nature Climate Change*, *7*(1), 58–62. https://doi.org/10.1038/nclimate3180

MacAyeal, D. R., & Sergienko, O. (2013). The flexural dynamics of melting ice shelves. *Annals of Glaciology*, *54*(63). https://doi.org/10.3189/2013AoG63A256

MacAyeal, D. R., Sergienko, O. V., & Banwell, A. F. (2015). A model of viscoelastic ice-shelf flexure. *Journal of Glaciology*, *61*(228), 635–645. https://doi.org/10.3189/2015JoG14J169

Mellor, M. (1960). Antarctic ice terminology: Ice dolines. *Polar Record*, *10*(64), 92. https://doi.org/10.1017/S0032247400050786

Mellor, M., & McKinnon, G. (1960). The Amery Ice Shelf and its hinterland. *Polar Record*, *10*(64), 30–34. https://doi.org/10.1017/s0032247400050579

Moore, J. (1993). Ice blisters and ice dolines. *Journal of Glaciology*, *39*(133), 714–716. https://doi.org/10.3189/s002214300001666x

Mosbeux, C., Wagner, T. J., Becker, M. K., & Fricker, H. A. (2020). Viscous and elastic buoyancy stresses as drivers of ice-shelf calving. *Journal of Glaciology*, *66*(258), 643–657. https://doi.org/10.1017/jog.2020.35

Moussavi, M., Pope, A., Halberstadt, A. R. W., Trusel, L. D., Cio, L., & Abdalati, W. (2020). Antarctic supraglacial lake detection using Landsat 8 and Sentinel-2 imagery: Toward continental generation of lake volumes. *Remote Sensing*, *12*(1), 134. https://doi.org/10.3390/rs12010134

Neumann, T. A., Brenner, A., Hancock, D., Robbins, J., Saba, J., Harbeck, K., et al. (2020). ATLAS/ICESat-2 L2A global geolocated photon data, version 3. Boulder, Colorado USA. NASA National Snow and Ice Data Center Distributed Active Archive Center. https://doi.org/10.5067/ATLAS/ATL03.003 [Accessed September 2020]

Neumann, T. A., Martino, A. J., Markus, T., Bae, S., Bock, M. R., Brenner, A. C., et al. (2019). The Ice, Cloud, and Land Elevation Satellite–2 mission: A global geolocated photon product derived from the Advanced Topographic Laser Altimeter System. *Remote Sensing of Environment*, *233*, 111325. https://doi.org/10.1016/j.rse.2019.111325

Noh, M. J., & Howat, I. M. (2017). The surface extraction from TIN based search-space minimization (SETSM) algorithm. *ISPRS Journal of Photogrammetry and Remote Sensing*, *129*, 55–76. https://doi.org/10.1016/j.isprsjprs.2017.04.019

Phillips, H. A. (1998). Surface meltstreams on the Amery Ice Shelf, East Antarctica. *Annals of Glaciology*, *27*, 177–181. https://doi.org/10.3189/1998aog27-1-177-181

Pope, A., Scambos, T., Moussavi, M., Tedesco, M., Willis, M., Shean, D., & Grigsby, S. (2016). Estimating supraglacial lake depth in West Greenland using Landsat 8 and comparison with other multispectral methods. *The Cryosphere*, *10*, 15–27. https://doi.org/10.5194/tc-10-15-2016

Rignot, E., Casassa, G., Gogineni, P., Krabill, W., Rivera, A., & Thomas, R. (2004). Accelerated ice discharge from the Antarctic Peninsula following the collapse of Larsen B ice shelf. *Geophysical Research Letters*, *31*, L18401. https://doi.org/10.1029/2004GL020697

Robel, A. A., & Banwell, A. F. (2019). A speed limit on ice shelf collapse through hydrofracture. *Geophysical Research Letters*, *46*(21), 12092–12100. https://doi.org/10.1029/2019gl084397

Scambos, T., Hulbe, C., & Fahnestock, M. (2003). Climate-induced ice shelf disintegration in the Antarctic Peninsula. In E. Domack, A. Leventer, A. Burnett, R. Bindschadler, P. Convey, & M. Kirby (Eds.), *Antarctic Peninsula Climate Variability: Historical and Paleoenvironmental Perspectives*, Antarctic Research Series (Vol. 79, pp. 79–92). https://doi.org/10.1029/AR079p0079

Schmeltz, M., Rignot, E., & MacAyeal, D. (2002). Tidal flexure along ice-sheet margins: Comparison of InSAR with an elastic-plate model. *Annals of Glaciology*, *34*, 202–208. https://doi.org/10.3189/172756402781818049

Smith, B., Fricker, H. A., Gardner, A., Siegfried, M. R., Adusumilli, S., Csathó, B. M., et al., & the ICESat-2 Science Team. (2020). ATLAS/ICESat-2 L3A land ice height, version 3. Boulder, Colorado USA. NASA National Snow and Ice Data Center Distributed Active Archive Center. https://doi.org/10.5067/ATLAS/ATL06.003 [Accessed September 2020]

Smith, B., Fricker, H. A., Holschuh, N., Gardner, A. S., Adusumilli, S., Brunt, K. M., et al. (2019). Land ice height-retrieval algorithms for NASA's ICESat-2 photon-counting laser altimeter. *Remote Sensing of the Environment*, *233*, 111352. https://doi.org/10.1016/j.rse.2019.111352

Spergel, J. J., Kingslake, J., Creyts, T., van Wessem, M., & Fricker, H. A. (2021). Surface meltwater drainage and ponding on Amery Ice Shelf, East Antarctica, 1973–2019. *Journal of Glaciology*, 1–14. https://doi.org/10.1017/jog.2021.46

Swithinbank, C. (1988). Antarctica. *Satellite image atlas of glaciers of the world*, United States Geological Survey Professional Paper 1386-B. Washington, DC: United States Government Printing Office.

Thomas, R. H. (1979). The dynamics of marine ice sheets. *Journal of Glaciology*, *24*(90), 167–177. https://doi.org/10.3189/s0022143000014726

Trusel, L. D., Frey, K. E., Das, S. B., Karnauskas, K. B., Munneke, P. K., Van Meijgaard, E., & van den Broeke, M. R. (2015). Divergent trajectories of Antarctic surface melt under two twenty-first-century climate scenarios. *Nature Geoscience*, *8*(12), 927–932. https://doi.org/10.1038/ngeo2563

van den Broeke, M. (2005). Strong surface melting preceded collapse of Antarctic Peninsula ice shelf. *Geophysical Research Letters*, *32*(12), L12815. https://doi.org/10.1029/2005GL023247

Vaughan, D. G. (1995). Tidal flexure at ice shelf margins. *Journal of Geophysical Research: Solid Earth*, *100*(B4), 6213–6224. https://doi.org/10.1029/94JB02467

Weertman, J. (1973). Can a water-filled crevasse reach the bottom surface of a glacier? *Hydrology of Glaciers, Cambridge Symposium 1969*, International Association of Hydrological Sciences (IAHS) Publication, (Vol. 95, pp. 139–145).

Yang, K., & Smith, L. C. (2016). Internally drained catchments dominate supraglacial hydrology of the southwest Greenland Ice Sheet. *Journal of Geophysical Research: Earth Surface*, *121*(10), 1891–1910. https://doi.org/10.1002/2016jf003927